

Article

GPM Annual and Daily Precipitation Data for Real-Time Short-Term Nowcasting: A Pilot Study for a Way Forward in Data Assimilation

Kaiyang Wang¹, Lingrong Kong², Zixin Yang¹, Prateek Singh¹ , Fangyu Guo¹, Yunqing Xu³, Xiaonan Tang¹ 
and Jianli Hao^{1,*} 

¹ Department of Civil Engineering, Xi'an Jiaotong-Liverpool University, Suzhou 215123, China; kaiyang.wang20@student.xjtlu.edu.cn (K.W.); zixin.yang20@student.xjtlu.edu.cn (Z.Y.); p.singh@xjtlu.edu.cn (P.S.); fangyu.guo@xjtlu.edu.cn (F.G.); xiao.tang@xjtlu.edu.cn (X.T.)

² Department of Planning, Wujiang Water Bureau, Wujiang District, Suzhou 215200, China; konglr2010@163.com

³ Department of Urban Planning and Design, Xi'an Jiaotong-Liverpool University, Suzhou 215123, China; yunqing.xu@xjtlu.edu.cn

* Correspondence: jianli.hao@xjtlu.edu.cn

Abstract: This study explores the quality of data produced by Global Precipitation Measurement (GPM) and the potential of GPM for real-time short-term nowcasting using MATLAB and the Short-Term Ensemble Prediction System (STEPS). Precipitation data obtained by rain gauges during the period 2015 to 2017 were used in this comparative analysis. The results show that the quality of GPM precipitation has different degrees of efficacy at the national scale, which were revealed at the performance analysis stage of the study. After data quality checking, five representative precipitation events were selected for nowcasting evaluation. The GPM estimated precipitation compared to a 30 min forecast using STEPS precipitation nowcast results, showing that the GPM precipitation data performed well in nowcasting between 0 to 120 min. However, the accuracy and quality of nowcasting precipitation significantly reduced with increased lead time. A major finding from the study is that the quality of precipitation data can be improved through blending processes such as kriging with external drift and the double-kernel smoothing method, which enhances the quality of nowcast over longer lead times.

Keywords: rainfall; satellite precipitation; GPM; hydroclimatic changes; nowcasting; STEPS; Mexico



Citation: Wang, K.; Kong, L.; Yang, Z.; Singh, P.; Guo, F.; Xu, Y.; Tang, X.; Hao, J. GPM Annual and Daily Precipitation Data for Real-Time Short-Term Nowcasting: A Pilot Study for a Way Forward in Data Assimilation. *Water* **2021**, *13*, 1422. <https://doi.org/10.3390/w13101422>

Academic Editors: Renato Morbidelli and David Dunkerley

Received: 9 March 2021

Accepted: 6 May 2021

Published: 20 May 2021

Publisher's Note: MDPI stays neutral with regard to jurisdictional claims in published maps and institutional affiliations.



Copyright: © 2021 by the authors. Licensee MDPI, Basel, Switzerland. This article is an open access article distributed under the terms and conditions of the Creative Commons Attribution (CC BY) license (<https://creativecommons.org/licenses/by/4.0/>).

1. Introduction

Precipitation is regarded as an essential component of global energy and water cycles, and it plays a significant role in the interactions between atmosphere, biosphere and hydrosphere [1]. The measurement of precipitation not only provides essential information to weather forecasters and climate scientists but also to a wide range of decision-makers, including agriculturalists, hydrologists, industrialists and emergency managers [2]. Therefore, accurate estimation and prediction of precipitation is important for a wide range of applications, such as agricultural crop forecasting, monitoring freshwater resources and numerical weather prediction. In the last three decades, satellite measurement of precipitation has grown to be an uninterrupted, reliable and cost-effective source over large data-void areas [3]. In 1997, NASA sent the first dedicated meteorological precipitation satellite—the Tropical Rainfall Measurement Mission (TRMM) Multi-satellite Precipitation Analysis (TMPA)—with the National Space Development Agency (NASDA) to measure energy and precipitation exchange across tropical and subtropical areas of the world for 17 years (1997–2014) [4,5]. Motivated by the splendid success of the TRMM satellite, on 27 February 2014, its successor, the GPM Core Observatory (GPMCO) was launched by

Japan Aerospace Exploration Agency (JAXA) and NASA to continue and improve satellite-based precipitation observations on a global scale [6]. Thanks to the other satellites, the Core satellite is possible to guarantee a covering region between 65° N and 65° S.

The GPM mission includes a constellation of nine satellites unified by the GPMCO as a reference standard for the other partner satellites [7]. The GPMCO contains an advanced 13-channel passive microwave radiometer, and a GPM Microwave Imager (GMI) combined with a Ka/Ku-band Dual-frequency Precipitation Radar (DPR). Since this radar has two frequencies that provides more accurate corrections for microwave rain attenuation, it unifies precipitation estimates as a benchmark [8]. Compared to the TRMM Precipitation Radar (PR), the DPR Ka-band is more sensitive for high-latitude snowfall and light rainfall (sensitivity of PR and Ka-band is 0.5 mm/h and 0.2 mm/h, respectively) [9]. Therefore, GPM DPR can more accurately detect extreme precipitation and estimate its impact on global climate models, which is essential for exploring and understanding the global water cycle [10].

In late 2014, precipitation from Integrated Multi-satellite Retrievals for GPM (IMERG) were released to the public; this especially high-resolution precipitation product is now available at the 30 min and 0.1° resolution in early mode (with a 4 h latency), late mode (with a 12 h latency) and final mode (with a 2.5 months latency), which run based on accuracy and latency [11]. The early and late products are multi-satellite data. The final run is, instead, obtained taking advantage of a combination of information acquired from satellite and monthly rain gauges data. Huffman et al. [12] suggested that this product can be regarded as the next generation of multi-sensor precipitation data and utilized for near real-time flood risk monitoring applications. Currently, some studies have utilized the IMERG products to estimate snowfall [11,13]. The potential of data from IMERG for real-time short-term rainfall nowcasting and forecasting are less unexplored due to the lack of reliable ground rain gauge observations. Therefore, the rainfall nowcasting and forecasting by IMERG data should be investigated with a view to improving the forecasting of extreme rainfall events and assessing the potential of feeding this information into hydrological models, especially in regions where high-resolution precipitation data is not available. Gilewski and Nawalany [14] suggested that precipitation nowcasting is the generation of short-term (0–3 h) future precipitation distributions from a sequence of radar images, while Xinjian et al. [15] claimed that the goal of precipitation nowcasting is to predict the future rainfall intensity in a local region over a short period of time. Nowcasting models are based on the extrapolation of radar rainfall scans to track the motion of precipitation cells with a forecasting lead time of a few hours. Quantitative precipitation estimation and precipitation nowcasting will help reduce or manage precipitation-related disasters such as flash-flooding [16], seasonal flooding [17], storms [18] and landslides [19]. Therefore, both precipitation measuring and predicting are significant for hydrology applications.

Using rain gauge data available from the Mexico Meteorological Services, this study applied a nowcasting model to compare the efficacy and reliability of precipitation data generated by GPM IMERG with ground data. The results provide valuable information, not only for improving the processes of satellite precipitation retrieval but also for operators in many relevant applications, from hydrological modelling and hazard research to climatic change-based simulations such as for flash flood forecasting in urban areas. The aim of this study was to investigate whether real-time short-term (0–6 h) satellite rainfall measurements can be applied effectively for nowcasting and forecasting of precipitation (rainfall) in developing countries. The research objectives are in three-folds: (1) to determine the efficacy and reliability of GPM precipitation compared to rain gauge data; (2) to assess the ability of nowcasting to forecast rainfall events with GPM rainfall; and (3) to gather evidence to show that GPM precipitation data can be used for real-time short-term forecasting.

To achieve the objectives, the STEPS (Short Term Ensemble Prediction System) nowcasting model was used to investigate the potential of GPM IMERG precipitation data and predict short-term real-time precipitation (0–3 h). The short duration analysis is justified

due to the fact that the resolution of weather radar is typically 1 km by 1 km, which is the most commonly used in nowcasting modelling. It was therefore necessary to use MATLAB projection for the GPM data in order to improve the accuracy of nowcasting results; the code developed by Liguori and Rico-Ramirez [20] was used for this purpose. After data projection, the resolution of the GPM data was corrected from 10 km by 10 km to 5 km by 5 km, which is the least resolution for GPM data without reducing the accuracy of the data. Several representative precipitation events (i.e., heavy rainfall for a day) in Mexico were then selected to simulate and nowcast precipitation. Finally, the performance of precipitation nowcasting was evaluated by calculating the errors between the observed precipitation and the nowcast results.

2. Latest Developments

Several studies have assessed the quality of the rainfall products of GPM missions when estimating global precipitation and the performance of precipitation nowcasting. At present, point measurements using a rain gauge and disdrometer [21,22], ground-based weather radar [23] and satellite-based sensors [24] are the most widely used techniques to measure and estimate precipitation. In most regions, tipping bucket rain gauges are frequently utilized to measure precipitation. Several studies demonstrated that tipping bucket rain gauge measurements are the most reliable technique in terms of point ground measurements [25–27]. However, they cannot measure quantities of precipitation less than 0.1 or 0.2 mm, depending on the size of the bucket [28]. Thus, depending on the intensity of rainfall measured, the tipping bucket rain gauges perform a temporal integration over a more or less long period. By contrast, ground weather radars have a large volume sample but present an indirect observation [23]. In terms of radar observations (also known as a remote sensing instrument), the reflectivity of precipitation at a given altitude is measured to estimate precipitation. The ground weather radar is able to supply rainfall rate data with a fine spatiotemporal resolution, but it is hindered by several limitations. For instance, the poor data management and archiving, difficult image data processing and usage is limited for weather forecasting [29]. Although ground weather radar can provide sound spatial resolutions to relatively large precipitation areas, the accuracy of radar precipitation estimates is affected by several sources of uncertainties and errors. For example, the radar signal attenuation and stability of radar calibration can affect the radar reflectivity measurement because of contamination of heavy precipitation by range effects or non-meteorological echoes (e.g., ground clutter) [30].

For satellite precipitation estimates, sensors onboard low-orbiting satellites are the only instruments able to retrieve global and homogeneous measurements of precipitation [31]. After the satellite measurement of radiances, the approaches applied to derive precipitation from radiances have advanced from Infrared (IR)- and Visible (VIS)-based methods to active and passive Microwave (MW) techniques and merged MW and IR methods [31]. In terms of active microwave sensors, Ku-band TRMM Precipitation Radar (PR) was the first spaceborne precipitation radar and has operated since 1997 [32]. The goal of TRMM satellite was to measure moderate to heavy precipitation to give a better understanding of the precipitation distribution on Earth and conduct near-real-time precipitation products. Since then, many methods such as [33–35] have built upon the success of the TRMM, culminating in the GPM mission. The Integrated Multi-Satellite Retrievals for GPM (IMERG) is the multi-satellite precipitation algorithm for GPM, which merges sparse precipitation estimates from IR-based geosynchronous satellites, all constellation microwave sensors and monthly gauge precipitation data [29]. NASA Goddard Earth Sciences (GES) Data and Information Services Center (DISC) produced the latest GPM IMERG version 5 (IMERG V5) precipitation dataset, which was employed in this study.

Compared to TRMM, GPM has improved temporal and spatial resolution, as well as a more efficient minimum latency time [31,36–38]. For example, Prakash et al. [36] compared both the TRMM TMPA (V7) and GPM IMERG (V03) with the rain gauge measurements over India. Their findings demonstrate that GPM provide more accurate information

about extreme rainfall events compared to TRMM. The IMERG data also presented a notable improvement over TMPA during the comparison with the rain gauge data in mountainous areas. Arshad et al. [37] compared both the GPM IMERG V05 data and the TRMM 3B42 V7 data with the rain gauge measurements over Pakistan. This work revealed that the performance of the IMERG final product showed the best results in the areas of higher annual average rainfall in terms of statistical indices (i.e., FAR, POD and CSI).

From Table 1 it can be obtained that the GPM satellite born precipitation data are available as near-real-time data available with a 4-h latency from acquisition and post-real-time research data, which are processed within 2.5 months.

Table 1. The key characteristics of GPM and TRMM.

Satellite Mission	Spatial Resolution	Temporal Resolution	Coverage	Minimum Latency	Period	Algorithm
GPM 'Early'	0.1°	0.5 h	65° S–65° N	4 h	2015-present	IMERG
GPM 'Late'				12 h		
GPM 'Final'				2.5 months		
TRMM	0.25°	3 h	50° S–50° N	9 h	1997–2015	Probability Matching

3. Methodology and Study Area

To evaluate the GPM IMERG, several steps were carried out, which are presented in Figure 1 below. The process started with the preparation of the rain gauge precipitation measurement data and the GPM data processing and preparation. The following step consisted of data comparison, which involved four major steps carried out by MATLAB processing [39], the last step of which was precipitation nowcasting of the observed GPM data by using the STEPS model. The STEPS nowcasting model is an available advanced Quantitative Precipitation Forecast (QPF) system, which was developed in the cooperation of the Australian Bureau of Meteorology and the UK MetOffice. A detailed mathematical description of the STEPS model can be found in [40,41]. The model generates ensembles of rainfall nowcasts by employing both the extrapolation of radar images and the downscaled rainfall output of Numerical Weather Prediction (NWP) models. The basis behind STEPS is to represent the uncertainty caused by the unpredictable rainfall growth and decay processes by adding stochastic perturbations to the deterministic extrapolation of radar images. The stochastic perturbations are designed to account for the unpredictable rainfall growth and decay processes and to reproduce the dynamic scaling of rainfall fields. Some studies have proved this model is reliable in several applications, such as prediction of flows in the sewer system [42] and hydrological forecasting in catchment [43].

The study area of this project is the whole of mainland Mexico, which is located at 23.626° N and 102.538° W in the southern portion of North America and covers a land surface area of 1964 million square kilometers [44]. The climate in Mexico is determined by different factors, such as latitude, elevation and ocean currents. As a result of its geographical location, the northern part of the country is located in a temperate area, while the southern part is in the inter-tropical area of the globe. Nearly two-thirds of the territory is considered semi-arid or arid, with annual precipitation lower than 500 mm, whereas one third is regarded as humid (the southeast), with precipitation of over 2000 mm per year [44]. Figure 2 shows the precipitation distribution in Mexico from 2010 to 2015 observed by ground weather radar, with more precipitation in the south of Mexico and less in the north during this period. The west coast of Mexico has a relatively low intense rainfall, while the east coast of Mexico has a relatively high intense rainfall, the details can be referred from [45]. This graph was used in this study as a reference for the GPM rainfall observations comparison. In most parts of Mexico, precipitation is more intense in the summertime when there is often torrential rain. Figure 3 presents the monthly average rainfall and temperature in the period of 1943 to 2018 over Mexico.

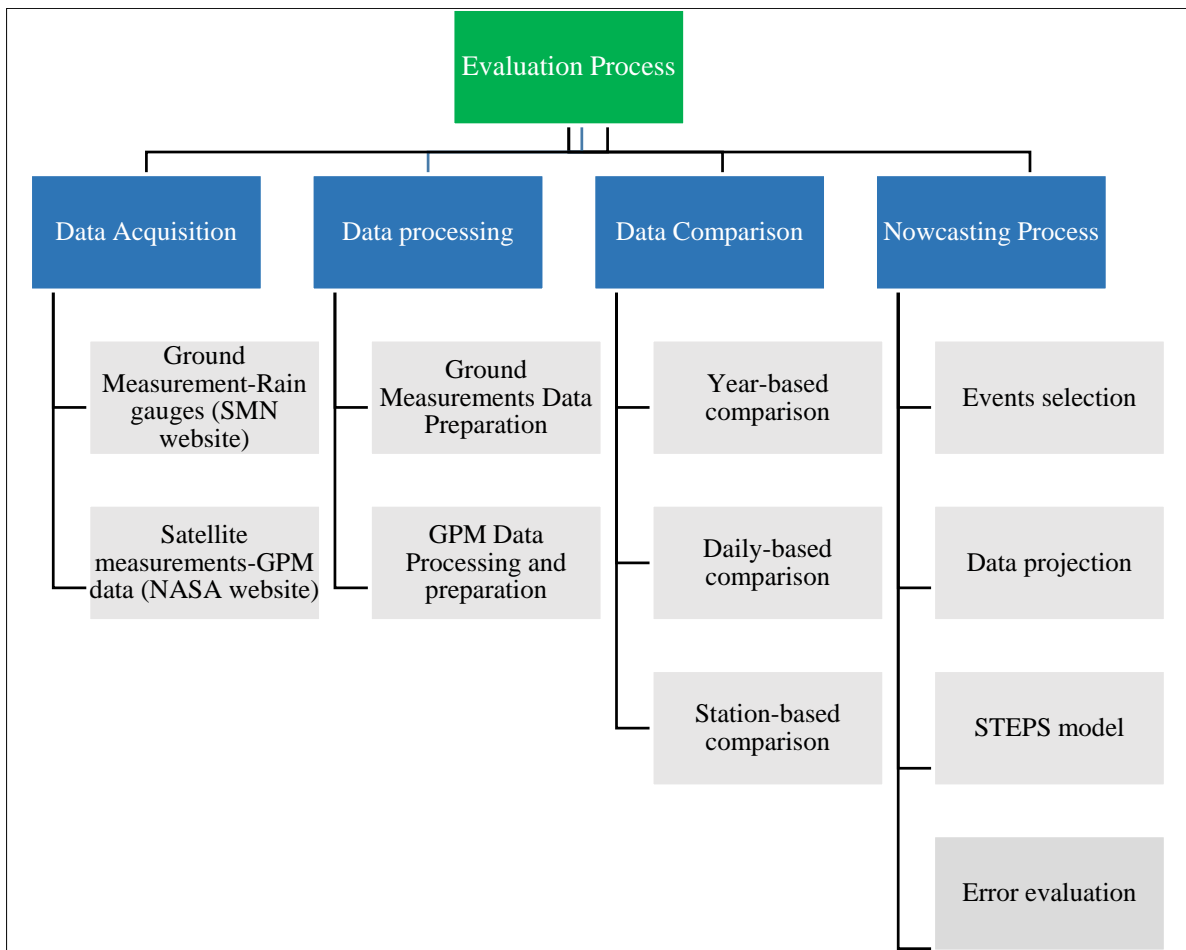


Figure 1. Flowchart of the evaluation process of the project.

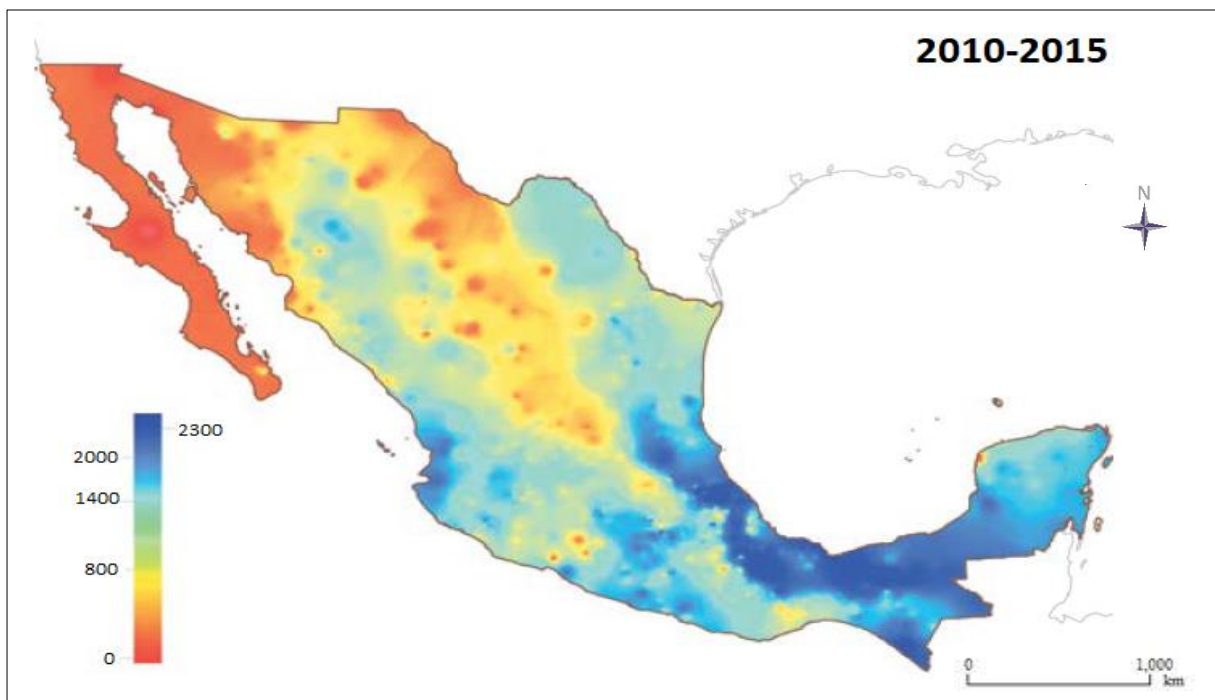


Figure 2. Maps showing the distribution of mean annual precipitation (mm) (2010–2015) (source: National Water Commission (CONAGUA)).

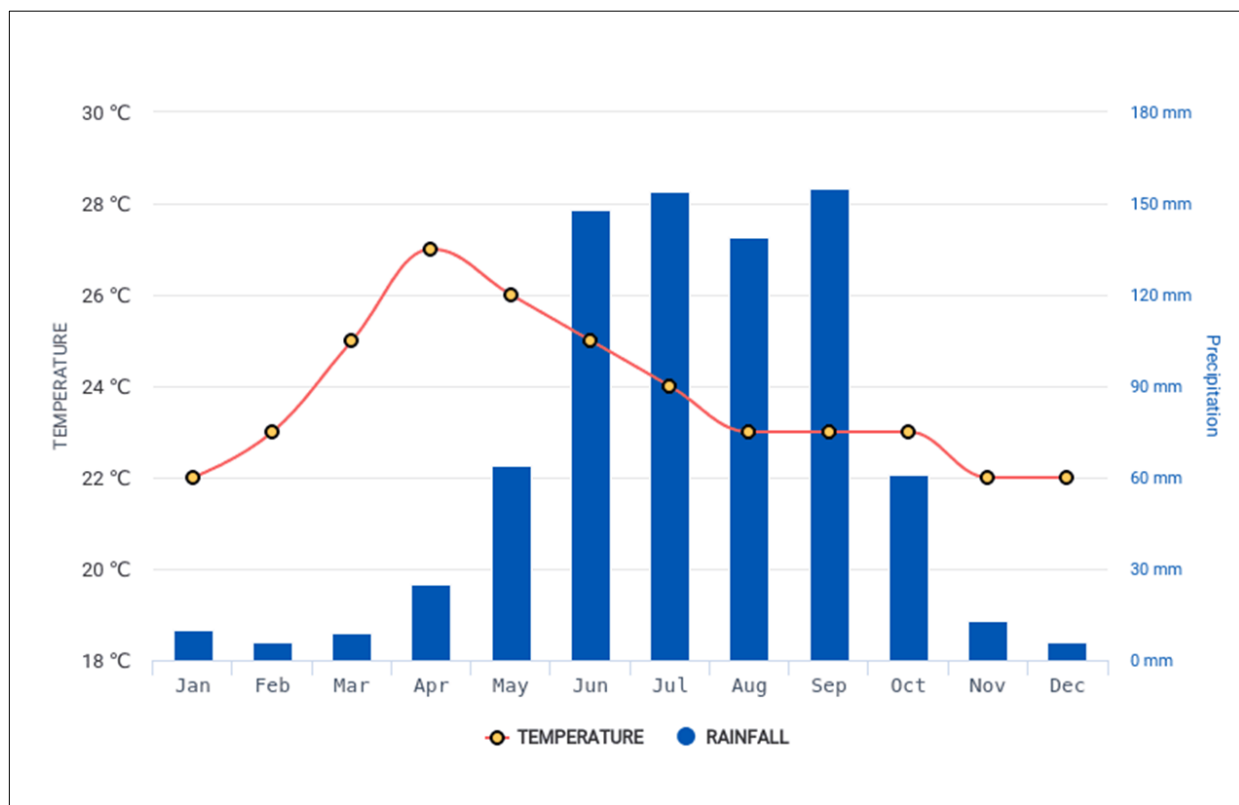


Figure 3. The monthly average rainfall and temperature in Mexico (1943–2018) (source: National Water Commission (CONAGUA)).

Rain gauge data was applied to provide a ground-based precipitation reference for GPM satellite data in this study. All rain gauge data in Mexico was collected through the online database provided by the Mexico National Meteorological Service website (<https://smn.conagua.gob.mx/es/>) accessed on 18 July 2019, which supply meteorological information and provides a quality-controlled dataset. The dataset consists of 2829 tipping bucket rain gauges, each with a temporal resolution of 24 h (UTC-6). From Figure 4 it can be observed that the distribution of rain gauges is uneven, which shows that the stations are accumulated densely in the south and spatially in the north. The reason for this is that the arrangement of rain gauges is based on the levels of precipitation density, so that there are more rain gauge stations in dense precipitation areas. This therefore reflects that southern Mexico receives more rainfall than the north. However, due to the frequency of measurement errors, traditional ground-based rain gauge measurements are not often regarded as a representative over large and high precipitation intensity areas, particularly at fine temporal resolutions. By contrast, satellite-based precipitation measurement has the potential to improve the understanding and forecasting of hydrological systems.

In this study, the GPM-IMERG V5 near-real-time (NRT) run product at 0.1° spatial resolution (around 10 km but varies from the equator to the poles) and 30 min temporal resolution were used. The data were available in an RT-H5 file format (RT indicates real-time and H5 represents an HDF5 file, respectively) and downloaded from the NASA Precipitation Measurement Program website (<http://www.pmm.nasa.gov>) accessed on 24 July 2019. In addition, the dataset was translated to the daily time period as to correspond with the rain gauge data set as only daily gauge precipitation data were available. Therefore, a daily period between 8 am to 8 pm local time (UTC-6) was created within the dataset by the MATLAB package. The data period collection of rain gauges and GPM IMERG is shown in Table 2 below.

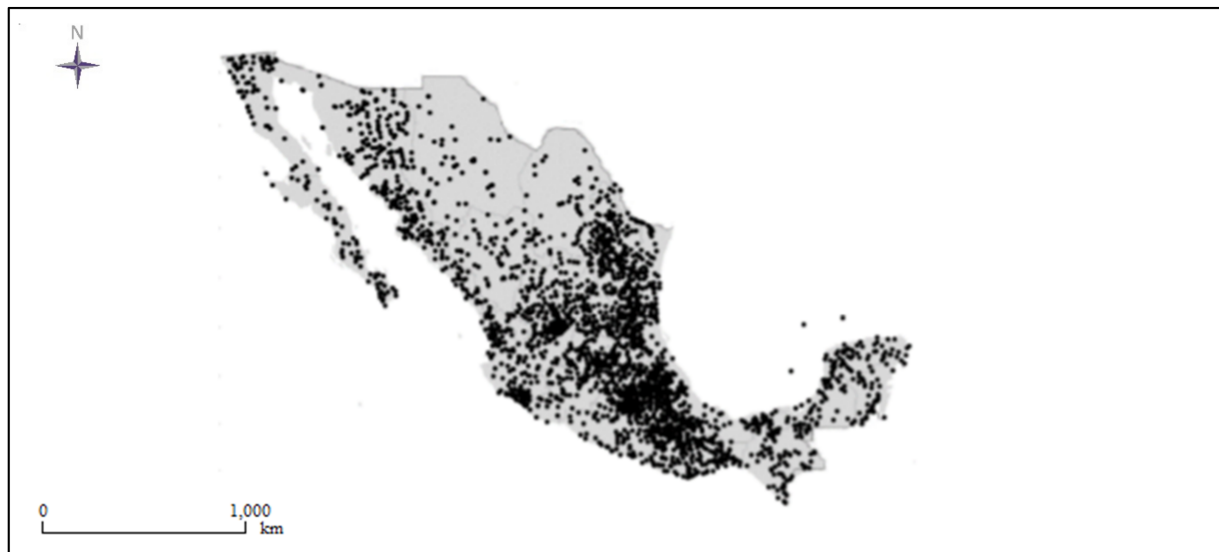


Figure 4. Distribution of rain gauge stations in Mexico (source: National Water Commission (CONAGUA)).

Table 2. Data period of rain gauges and GPM.

Observations	Start	End	Time Period
Rain gauges	1 June 1957	1 March 2018	24 h
GPM	1 June 2014	1 July 2018	24 h

From the table, it can be seen that the same period of data collection of rain gauges and GPM is from 1 June 2014 to 1 March 2018 and the full-year data for both of them are from 2015 to 2017. Therefore, the precipitation data from this period of three years (2015–2017) was used in this analysis. Since the collected data is unstructured from the website, the processing the raw data into structured data takes considerable time for post processing.

The distribution of mean annual precipitation in Mexico from 2010 to 2015 according to the National Water Commission (Figure 2), which was estimated by weather radar. In order to give a broad understanding of the quality of the GPM product for measuring precipitation over Mexico, Figure 5 was plotted by MATLAB to present the distribution of the mean annual precipitation estimated using GPM data over a three-year period from 2015 to 2017. By comparing these two graphs, it can be observed that the precipitation distribution estimated by GPM is quite close to the radar precipitation estimation, and the GPM is proven to be able to duplicate the spatial precipitation patterns while showing only slight overestimates in coastal areas. The preliminary analysis indicates that the quality of the GPM data performs well at the national scale.

After evaluating the quality of GPM data at the annual and national scales, it was found that the GPM presented a relatively high agreement with rain gauges. It needs to be noted that the rain gauge data with zero was ignored in this study. The next stage of the study investigated the quality of GPM data at the daily scale by using single and multiple gauges. For single gauges, three single rain gauge stations were chosen with different elevations above sea level based on two criteria: (a) the elevation is typical over Mexico, and (b) it has continuous data throughout the three-year period 2015–2017. Figure 6 presents the location of the selected three rain gauges, which are gauge 1084 at 2032 m elevation, gauge 25074 at 1472 m elevation and gauge 7038 at 226 m elevation. In addition, the climate around gauge 1084 has a dry winter, pleasantly warm during the day and a very hot summer. For gauge 25074, the climate is hot all year round, but the dry season, from November to May, is sunny and it almost never rains. For gauge 7038, the least rainy period runs from February to April, and the driest month is April.

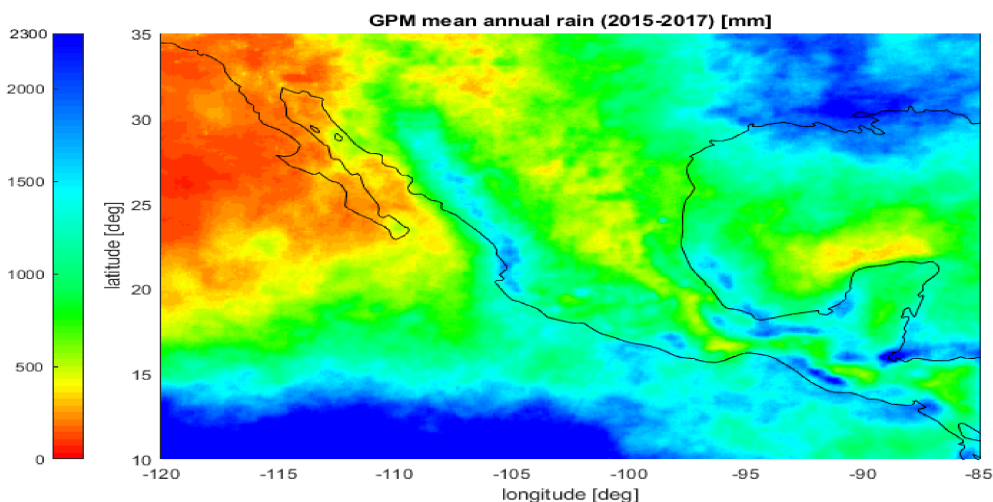


Figure 5. Map showing the distribution of mean annual precipitation in mm measured by GPM (2015–2017).



Figure 6. Location of the selected rain gauge stations in Mexico.

4. Data Processing

In order to detect and evaluate the quality and performance of GPM data, the rain gauge data was applied as a reference for comparison. Several conventional statistical performance metrics were selected, which were the Correlation Coefficient (CC) in Equation (1), the Mean Absolute Error (MAE) in Equation (5) [46], the Root Mean Square Error (RMSE) in Equation (4) [47,48] and the Relative Bias (BIAS) in Equation (6). Firstly, the CC described the agreement between satellite estimates and rain gauge observations, and secondly, the MAE, RMSE and BIAS was applied to describe the error and bias of satellite estimates compared with rain gauge observations [49]. The relevant equations are as follows [50,51]:

Pearson Correlation Coefficient (CC) was calculated as Equation (1):

$$CC = \frac{\frac{1}{n} \sum_{i=1}^n (P_S^{(i)} - \overline{P_S})(P_G^{(i)} - \overline{P_G})}{\sigma_S \sigma_G} \tag{1}$$

$$\sigma_S = \sqrt{\frac{1}{n} \sum_{i=1}^n (P_S^{(i)} - \bar{P}_S)^2} \quad (2)$$

$$\sigma_G = \sqrt{\frac{1}{n} \sum_{i=1}^n (P_G^{(i)} - \bar{P}_G)^2} \quad (3)$$

The Root Mean Square Error (RMSE) was obtained by Equation (4) as:

$$\text{RMSE} = \sqrt{\frac{\sum_{i=1}^n (P_S^{(i)} - P_G^{(i)})^2}{n}} \quad (4)$$

The Mean Absolute Error (MAE) was obtained by Equation (5) as:

$$\text{MAE} = \frac{\sum_{i=1}^n |P_S^{(i)} - P_G^{(i)}|}{n} \quad (5)$$

The GPM product overestimates precipitation amounts if MAE value higher than 1, otherwise, the satellite product underestimates the precipitation.

The Relative Bias (BIAS) was obtained by Equation (6) as:

$$\text{BIAS} = \frac{\sum_{i=1}^n (P_S^{(i)} - P_G^{(i)})}{\sum_{i=1}^n (P_G^{(i)})} \times 100\% \quad (6)$$

where P_G and P_S represent the actual precipitation value provided by rain gauges and precipitation estimation provided by the satellite product, respectively. n is regarded as the number of observations. σ_S and σ_G are standard deviations of GPM satellite precipitation and standard deviations of rain gauge precipitation, respectively.

In addition, in terms of probabilistic statistical indices, the probability of detection (POD), the critical success index (CSI) and the false alarm ratio (FAR) was applied to describe the eventuality of GPM satellite precipitation estimates. POD provides the fraction of precipitation events that the satellite distinguishes among all the actual precipitation events, and FAR provides the fraction of unreal events among all the events GPM satellites detect [49]. The CSI was essentially obtained by a function of POD and FAR. These equations were as follows [6,52]:

The Probability of Detection (POD) as Equation (7) as:

$$\text{POD} = \frac{n_{11}}{n_{11} + n_{01}} \quad (7)$$

The False Alarm Ratio (FAR):

$$\text{FAR} = \frac{n_{10}}{n_{11} + n_{10}} \quad (8)$$

The Critical Success Index (CSI):

$$\text{CSI} = \frac{n_{11}}{n_{11} + n_{01} + n_{10}} \quad (9)$$

where n_{11} represents precipitation observed by the rain gauge and GPM satellite simultaneously. n_{10} is precipitation observed by the GPM satellite but not observed by the rain gauge, and n_{01} is converse to n_{10} . The perfect values of the evaluation metrics are presented in Table 3 below [38,49]. Moreover, since the expression for precipitation intensity in this study is the collecting of precipitation over a consistent time period, the unit of precipitation is 'mm' instead of 'mm/h'.

Table 3. The range and perfect values of statistical performance measures.

Statistical Metrics	Unit	Perfect Value
Correlation Coefficient (CC)	N/A	1
Root Mean Square Error (RMSE)	mm	0
Mean Absolute Error (MAE)	mm	0
Relative Bias (BIAS)	N/A	1
Probability of Detection (POD)	N/A	1
False Alarm Ratio (FAR)	N/A	0
Critical Success Index (CSI)	N/A	1

5. Results and Discussion

5.1. Annual Precipitation

To explore the quality of GPM precipitation data, a comparison between the estimates from rain gauges and GPM was carried out based on data collected from 2015 to 2017. Figures 7 and 8 show the scatterplots of GPM IMERG satellite precipitation versus rain gauge data at annual scales over Mexico from 2015 to 2017.

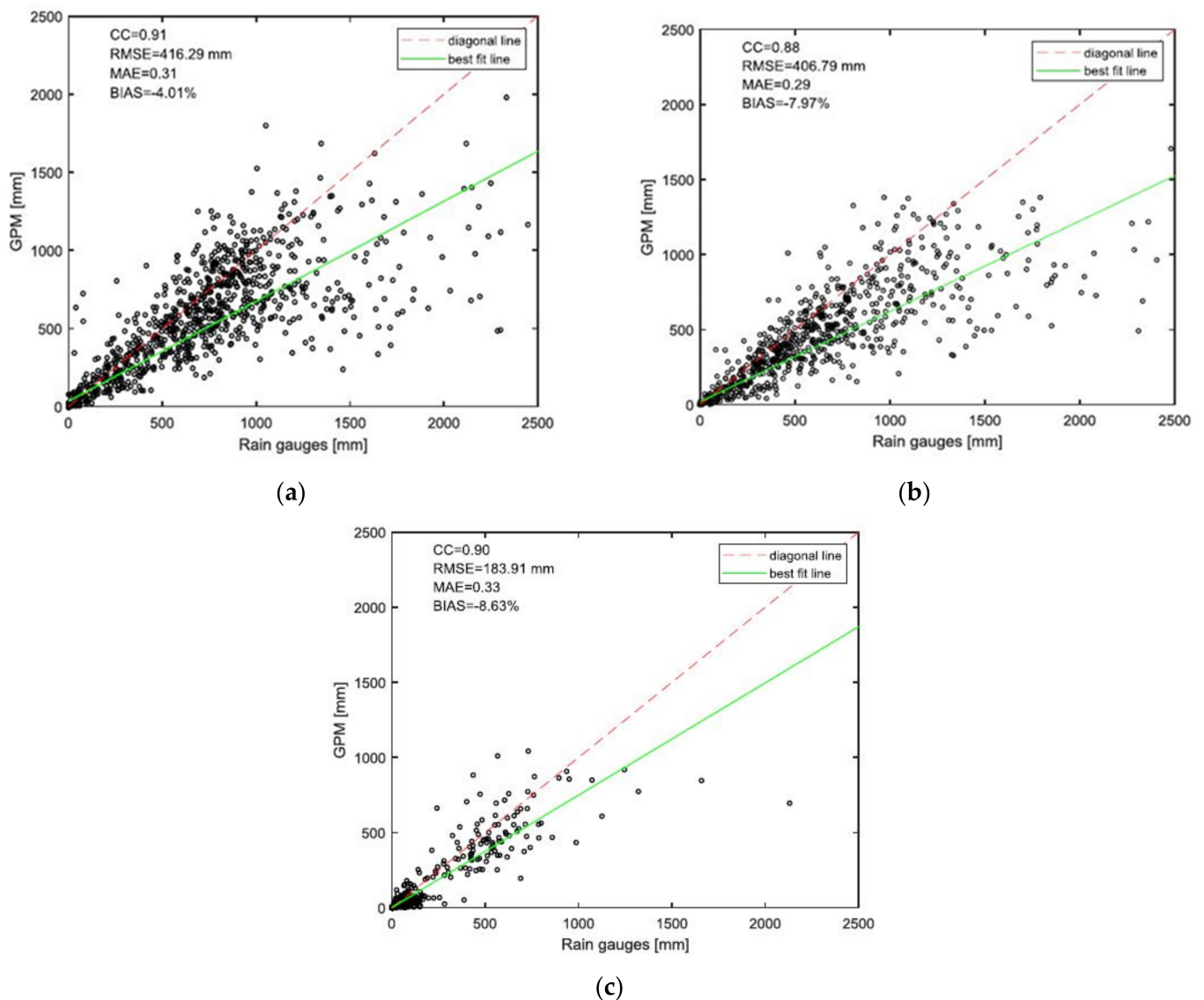


Figure 7. Comparison of the precipitation between GPM satellite and rain gauges in (a) 2015; (b) 2016; and (c) 2017 at annual scale.

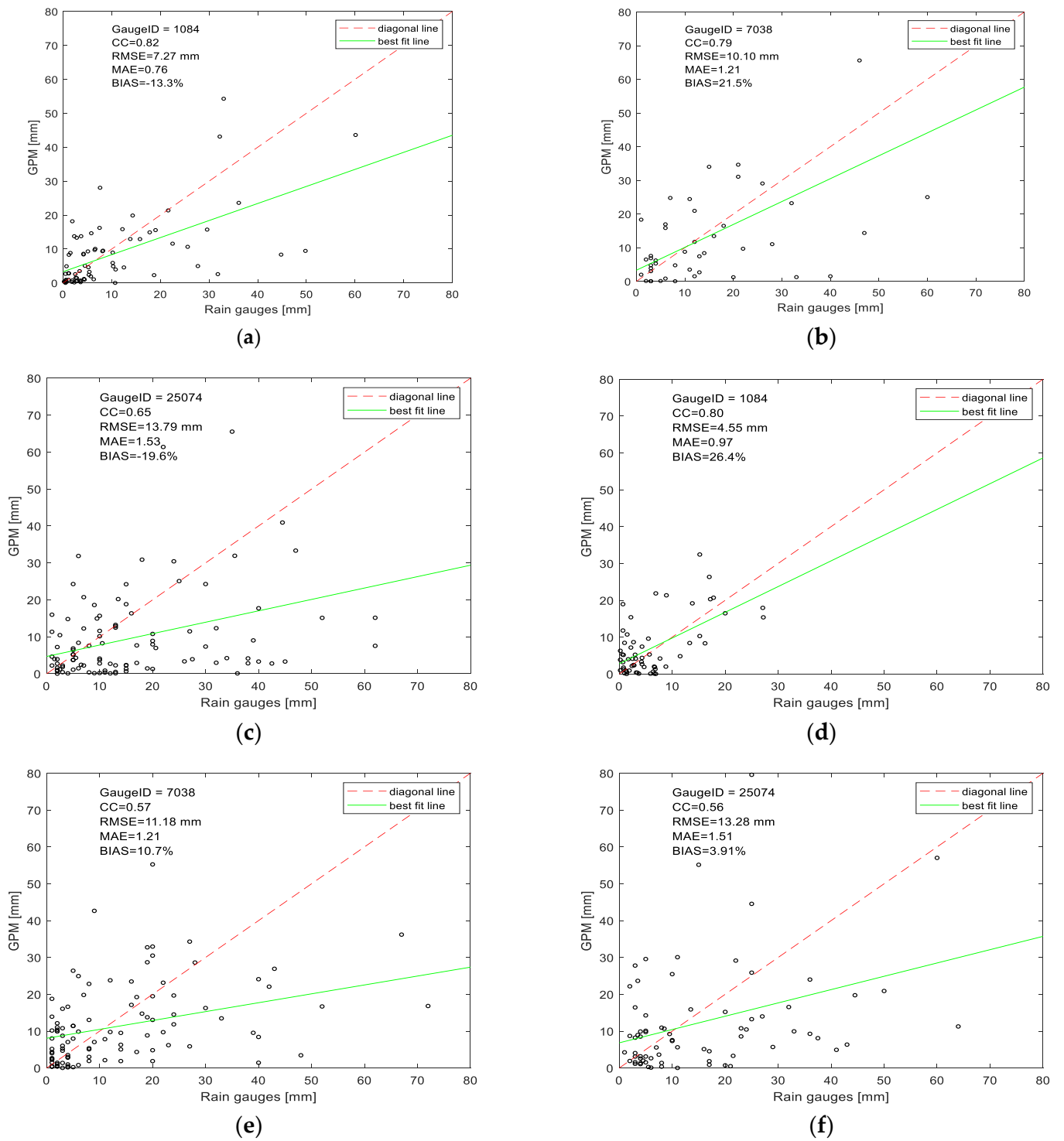


Figure 8. Cont.

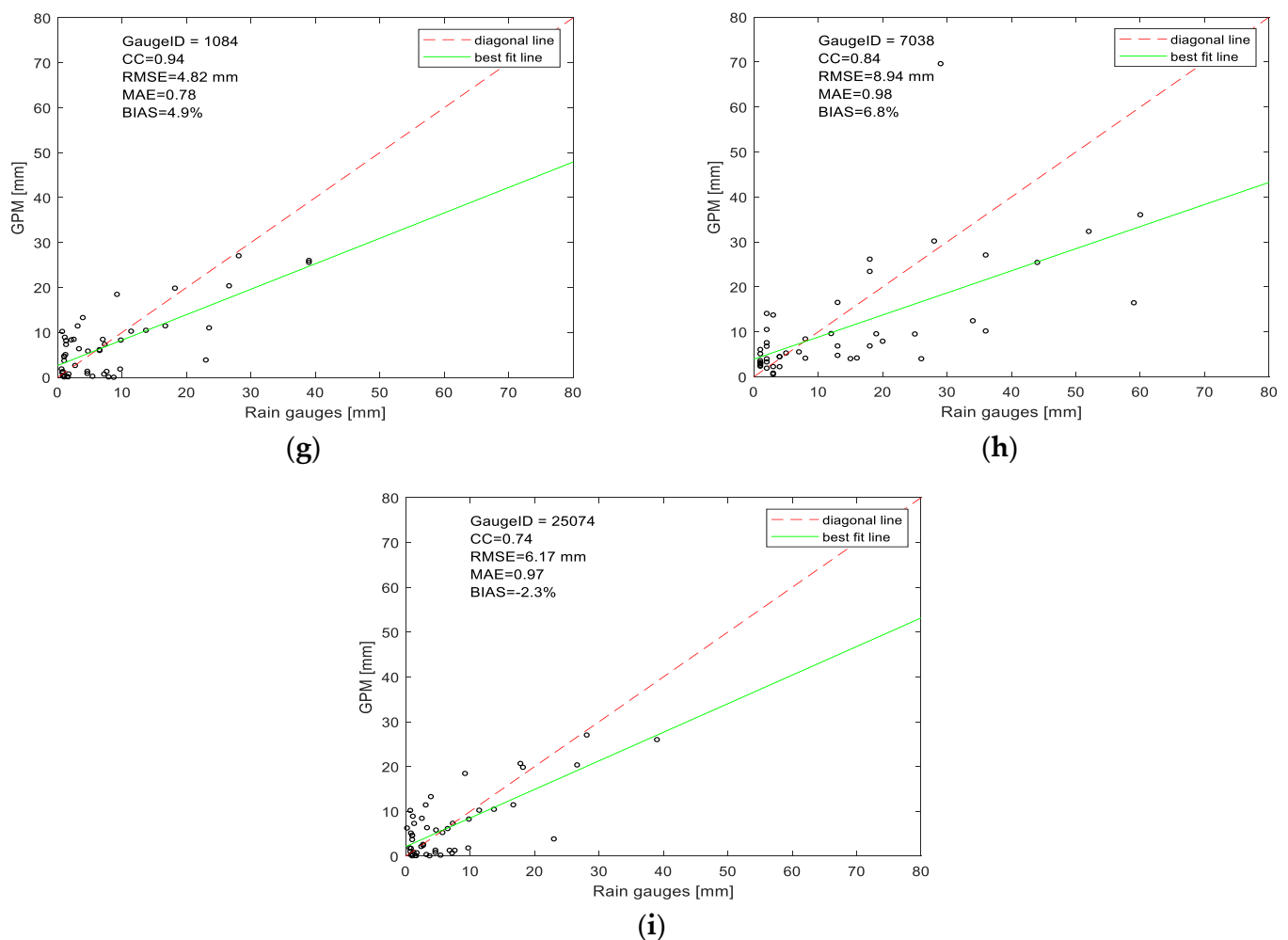


Figure 8. Comparisons of the daily precipitation for a single gauge between GPM and single gauge (a) gauge 1084 (b) gauge 7038 (c) gauge 25074 in 2015 (a–c); (d) gauge 1084 (e) gauge 7038 (f) gauge 25074 in 2016 (d–f); and (g) gauge 1084 (h) gauge 7038 (i) gauge 25074 in 2017 (g–i), respectively.

As can be observed, the conventional evaluation metrics are also indicated in these figures, and all the evaluation results are presented in Table 4. As mentioned before, the scale of the GPM data was projected into 5 km by 5 km since the STEPS model can process the data in the range from 5 km by 5 km to 1 km by 1 km. In theory, each graph should have 2829 points (one point for each station). As expected, GPM showed a relatively high degree of agreement with rain gauges at annual scales, because the values of CC are close to 1 (0.91, 0.88 and 0.90), which meets the finds by Liberto et al. [53] Similar study obtained the close CC results. However, there are significant gaps in the data points of 2017, as shown in Figure 7c, because the precipitation data for rain gauges in 2017 were missing for some gauge stations (perhaps due to maintenance). The RMSE for 2017 is therefore significantly lower than for the previous two years. The values of RMSE are 416.29 mm and 406.79 mm in 2015 and 2016, respectively. Furthermore, the GPM shows a slight underestimation of precipitation according to the BIAS value, which means that GPM generated negative errors (bias < 0); the greater the BIAS value is from 1, the more biased the data is. Thus, the BIAS is shown to have decreased from -4.01% to -8.63% between 2015 and 2017, which indicates the data for 2017 is more biased, and GPM is underestimating more. This may be because the GPM is not sensitive to light precipitation. In addition, the values of MAE fluctuated from 0.29 to 0.33 for the three years, with the lowest value in 2016 and the highest in 2017. In terms of probabilistic statistical evaluation metrics, the POD (0.73 to 0.86), FAR (0.19 to 0.25) and CSI (0.55 to 0.73) are very satisfying, indicating that GPM IMERG can

capture most precipitation events over Mexico. Due to the missing data for rain gauges in 2017, the POD, FAR and CSI are relatively bad. Overall, the results are acceptable and the GPM IMERG product is able to reproduce a mostly consistent distribution of precipitation at the annual scale.

Table 4. Summary of evaluation metrics for GPM IMERG product, which was calculated based on mean regional and national scale precipitation.

Scale	Year	CC	RMSE (mm)	MAE	BIAS (%)	POD	FAR	CSI
Regional	2015	0.91	416.29	0.31	−4.01	0.86	0.19	0.73
	2016	0.88	406.79	0.29	−7.97	0.82	0.22	0.62
	2017	0.90	183.91	0.33	−8.63	0.73	0.25	0.55
National	2015–2017	0.90	298.94	0.30	−6.87	0.79	0.21	0.70

In order to evaluate the performance of the GPM versus rain gauges at the national scale, Figure 9 presents the mean annual precipitation for the three-year period from 2015 to 2017, and the results of the evaluation metrics for GPM for the period 2015–2017 are shown in Table 4. From both, it can be seen that GPM present an underestimation of mean annual precipitation over Mexico, especially for the southern low altitude regions where observations of GPM can improve. Moreover, the value of CC of GPM IMERG was 0.90, which is in high agreement with the rain gauges, indicating that GPM can also capture temporal variations at the national scale. In addition, since POD (0.79), FAR (0.21) and CSI (0.70) were consistent, the GPM captured most precipitation events correctly.

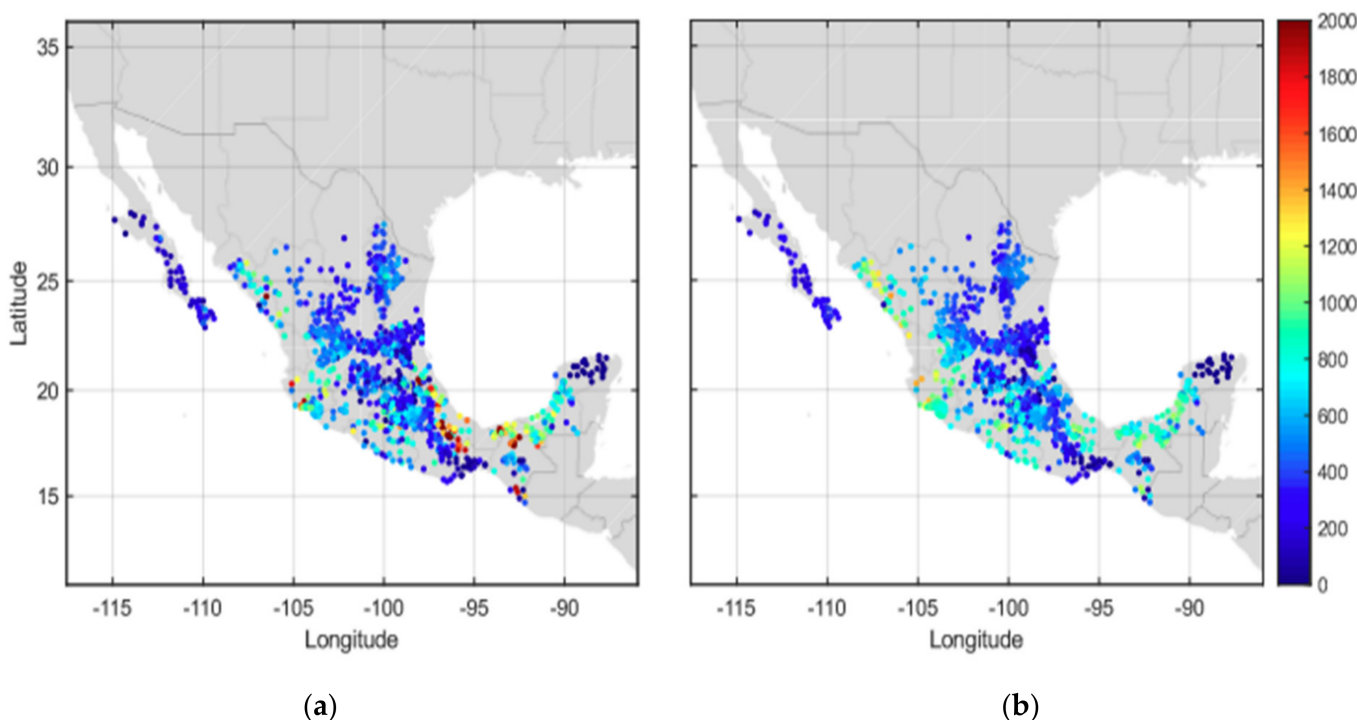


Figure 9. Mean annual precipitation measured by (a) rain gauges and (b) GPM (2015–2017).

To summarize, the performance of the GPM IMERG precipitation product is satisfactory at both annual and national scales but shows a slight underestimation due to most precipitation having happened in low-altitude sites or mistaken precipitation measurements by rain gauges.

5.2. Daily Precipitation

Figure 8a–i show the daily precipitation distributions for the chosen gauge stations for 2015–2017, respectively. Plots for each gauge should have 365 points in theory (one for each day of the year). However, some plots have fewer points than this because of the disproportionate temporal precipitation patterns in Mexico. Additionally, due to most precipitation falling in the summertime, there are many low values of precipitation throughout the rest of year, which is not easily visible on the graphs.

For gauge 1084 (Figure 8a,d,g), it can be observed that the values of CC (around 0.86) are high, which indicates that the precipitation data of GPM IMERG and rain gauges were in relatively high agreement compared to the other two single gauge stations. However, the CC values of gauge 25074 (Figure 8c,f,i) are relatively low at around 0.65. This can be explained by the fact that the precipitation intensity is high in that region, which can cause the measurement errors of surrounding rain gauges and result in a low agreement between GPM and gauge data. A similar study [52] was conducted in the Yangtze River basin at a daily scale, presenting a low CC value (0.44) between IMERG and rain gauge data. Furthermore, both of the values of RMSE and MAE for three gauges are acceptable in Table 5, which are mean value of 8.2 mm and 1.12, respectively. In terms of the values of BIAS, most of the values are positive, which indicate that the GPM precipitation product overestimated the precipitation, especially for gauge 7038. Nevertheless, the results show that the GPM precipitation measurements underestimated the precipitation at the national and annual scales. The reason may be because the precipitation intensity was relatively high on that day and the wind flow may have impacted the measurement of precipitation by rain gauges, a phenomenon revealed by the literature review. Thus, the precipitation exceeded the capability of rain gauge measurement, which resulted in the instrument error. For the probabilistic statistical indices (POD, FAR and CSI), the values varied by about 0.75–0.89, 0.21–0.31 and 0.68–0.73, respectively. Based on the results, it was found that the performance of the GPM IMERG precipitation product is decent at the daily scale. Moreover, in order to compare the precipitation data of GPM and rain gauges more clearly, Figure 10 was plotted to show the mean daily precipitation between GPM and rain gauges during the period of 2015–2017. Note that the red dash line indicates a year break. From the plot, it is clearly seen that the GPM and rain gauge profiles are in good agreement. The value of BIAS is -4.68% , so the GPM precipitation product shows a slight underestimation, and the values of RMSE and MAE are good at 2.36 mm and 0.94, respectively. The data quality of the GPM precipitation product is therefore high at the daily scale.

Table 5. Summary of evaluation metrics for GPM IMERG products at daily scale for single rain gauges.

Gauge ID	Elevation (m)	Time	CC	RMSE (mm)	MAE	BIAS (%)	POD	FAR	CSI
1084	2032	2015	0.82	7.27	0.76	−13.3	0.89	0.21	0.74
		2016	0.80	4.55	0.97	26.4	0.87	0.23	0.71
		2017	0.94	4.82	0.78	4.9	0.91	0.20	0.77
		Average	0.86	5.55	0.84	6.0	0.89	0.21	0.74
7038	226	2015	0.79	10.10	1.21	21.5	0.78	0.28	0.71
		2016	0.57	11.18	1.21	10.7	0.85	0.24	0.76
		2017	0.84	8.94	0.98	6.8	0.81	0.26	0.72
		Average	0.73	10.07	1.13	13.0	0.81	0.26	0.73
25074	1472	2015	0.65	13.79	1.53	−19.6	0.74	0.31	0.69
		2016	0.56	13.28	1.51	3.91	0.70	0.33	0.64
		2017	0.74	6.17	0.97	−2.3	0.80	0.28	0.70
		Average	0.65	11.08	1.34	−5.99	0.75	0.31	0.68

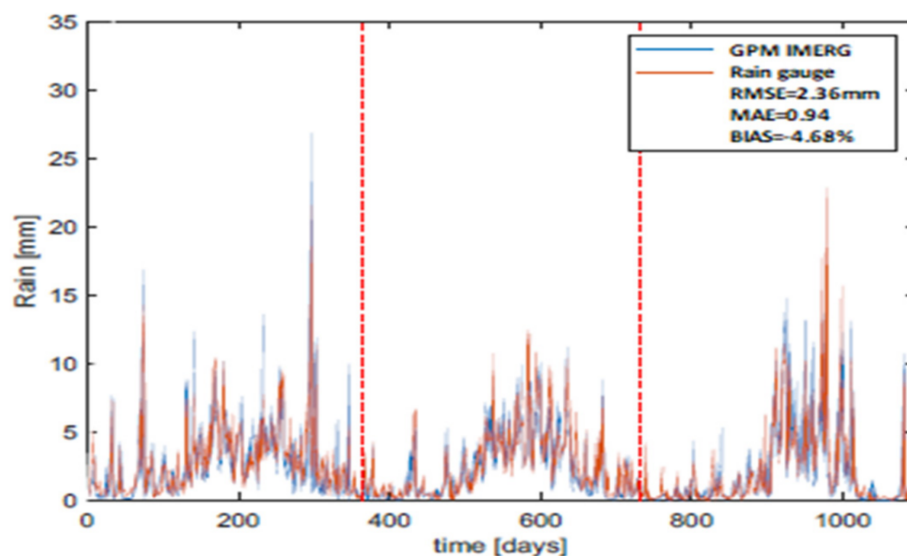


Figure 10. Mean daily precipitation (all gauge stations) between GPM and rain gauges (2015–2017).

6. Application of Precipitation Nowcasting

6.1. Events Selection

Normal monthly precipitation from 1943 to 2018 over Mexico (see Figure 3), as collected by the National Water Commission, was chosen as the representative precipitation events. It can be seen that the intensity of precipitation is relatively high during the months of June, July, August, September and October. Hence, based on the level of precipitation, five precipitation events were used in the STEPS model for precipitation nowcasting because a large number of precipitation events are more predictable [41]. Each precipitation event presented different characteristics in terms of date and type, as shown in Table 6.

Table 6. Dates and durations of selected rainfall events.

Event	Date	Time Period	
		Start	End
1	22 October 2015	01:00	24:00
2	17 June 2017	01:00	24:00
3	18 July 2017	01:00	24:00
4	1 August 2017	01:00	24:00
5	1 September 2017	01:00	24:00

After processing the GPM precipitation modified data by the STEPS model, the spatial distribution of the nowcast precipitation was obtained as shown in Figure 11. Figure 11a,b are the precipitation estimated by GPM and 30-min forecast precipitation from STEPS on 22 October 2015, respectively. They can be compared with each other to observe the actual and simulated precipitation cloud movements. Eleven figures for precipitation nowcasting from 1 h to 6 h are shown in Supplementary Materials. It can be clearly seen that the nowcast accuracy decreases rapidly with lead time, which was also found by PC et al. [54]. Please check Figures in Supplementary Materials for precipitation on 22 October 2015 from 9:30 to 14:30, based on (a) GPM estimated precipitation and (b) 30-min forecast precipitation from STEPS precipitation nowcast.

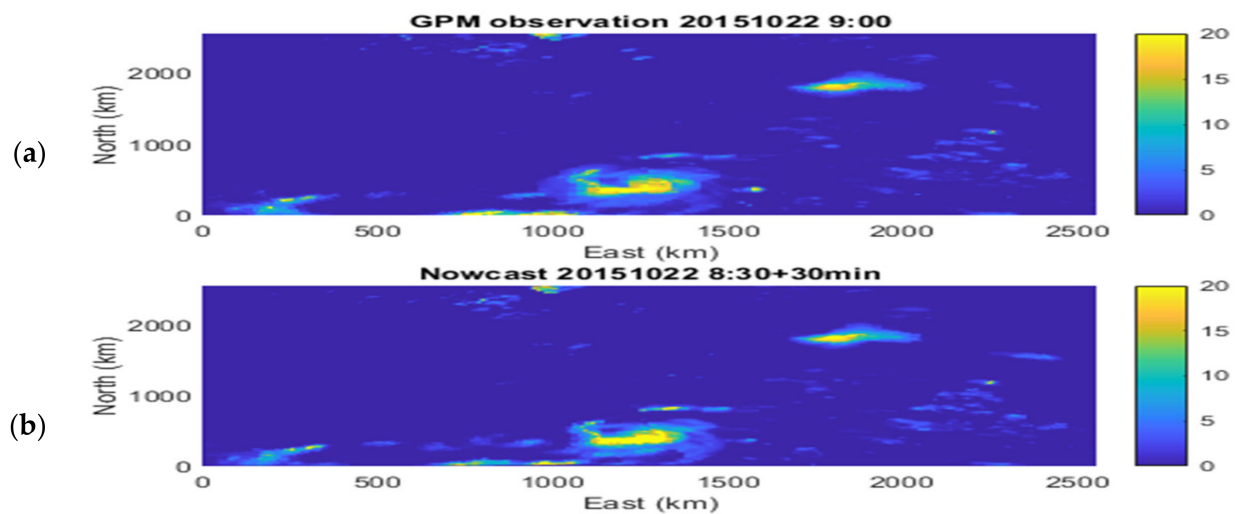


Figure 11. Precipitation on 22 October 2015 at 9:00, based on (a) GPM estimated precipitation and (b) 30-min forecast precipitation from STEPS precipitation nowcast.

6.2. Error Analysis

The RMSE, MAE, CC and BIAS were calculated between STEPS nowcast and GPM precipitation data at different lead times for each event, the profiles of which are shown in Figure 12a–d with their mean value lead times presented in Table 7. The average RMSE and MAE values between STEPS nowcast and GPM for five events during the whole period were obtained (7.1 mm and 4.2 mm, respectively), which indicate the errors related to the estimation of GPM precipitation. The results demonstrate that the errors obtained from the nowcast data are relatively small but increase with growing lead time, and that the errors of RMSE and MAE increase as the lead time increases. For CC and BIAS, both of them decreased with the increased lead time, and the accuracy of precipitation nowcasting decreases as the lead time grows, which concurs with finding of a previous study [55]. Overall, the trend of nowcast precipitation decreases as the lead time increases.

Table 7. Summary of evaluation metrics for GPM IMERG versus nowcasts results along the lead times.

Lead Times	RMSE	MAE	CC	BIAS
30	3.69	1.91	0.68	0.88
60	4.50	2.20	0.61	0.85
90	4.80	2.69	0.56	0.84
120	5.93	3.71	0.50	0.82
150	6.17	4.96	0.44	0.79
180	5.92	3.90	0.42	0.78
210	6.44	4.75	0.38	0.78
240	6.57	4.98	0.35	0.74
270	6.85	4.24	0.32	0.75
300	7.20	5.47	0.27	0.76
330	7.77	5.96	0.24	0.73
360	10.31	5.78	0.20	0.72

In order to investigate the variability of errors, box plots were produced as presented in Figure 13a–d. Box plots of errors of the GPM IMERG product provide details of the accuracy of nowcasting. The lower and upper edges of the central box are the third (75%) and first (25%) quantiles that represent the Interquartile Range (IQR), as the central inside band and cross sign represents the median and mean values, respectively [56].

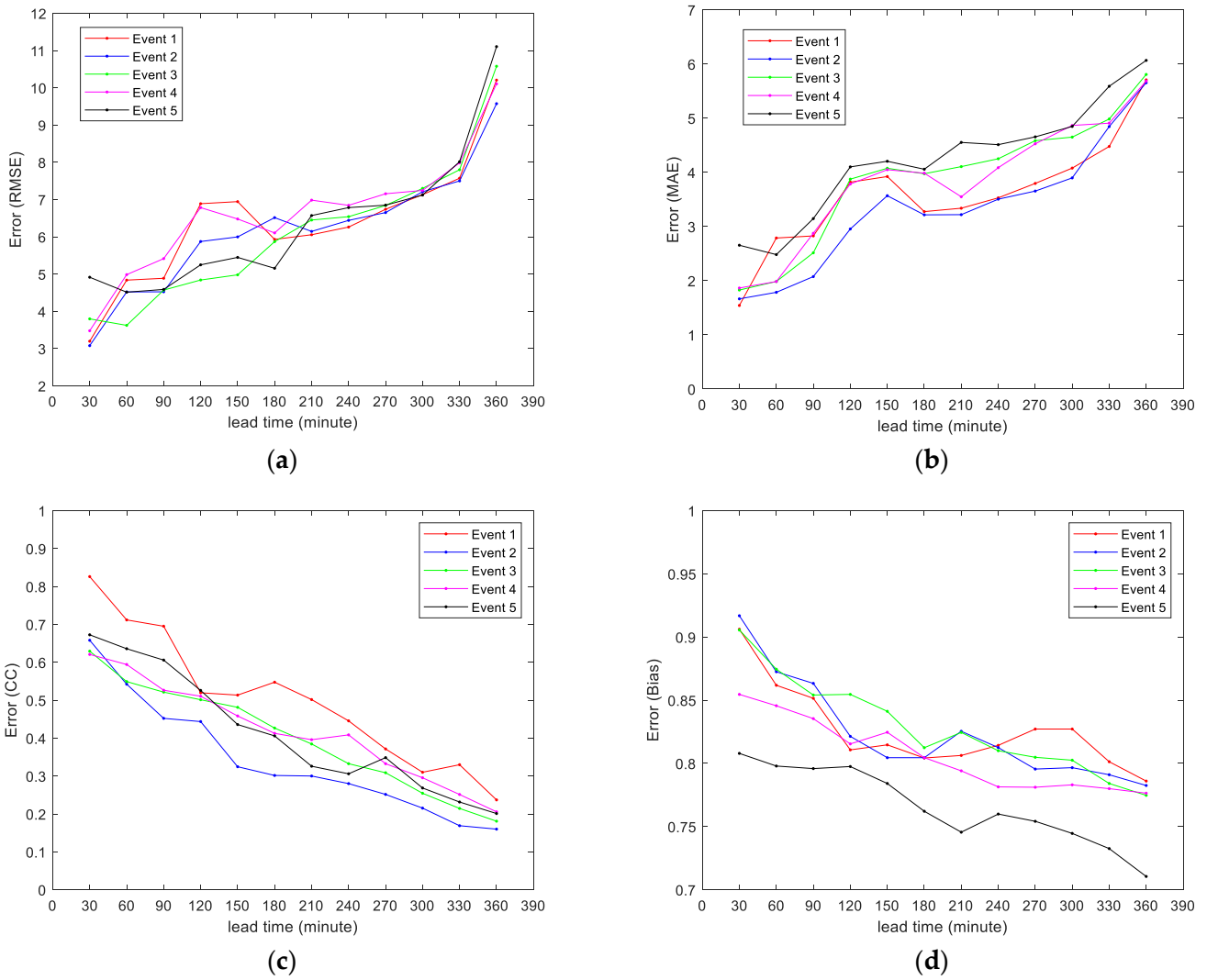


Figure 12. Summary of (a) root mean square error; (b) mean absolute error; (c) correlation coefficient; and (d) BIAS profiles from the five precipitation events, obtained by STEPS model at different lead times.

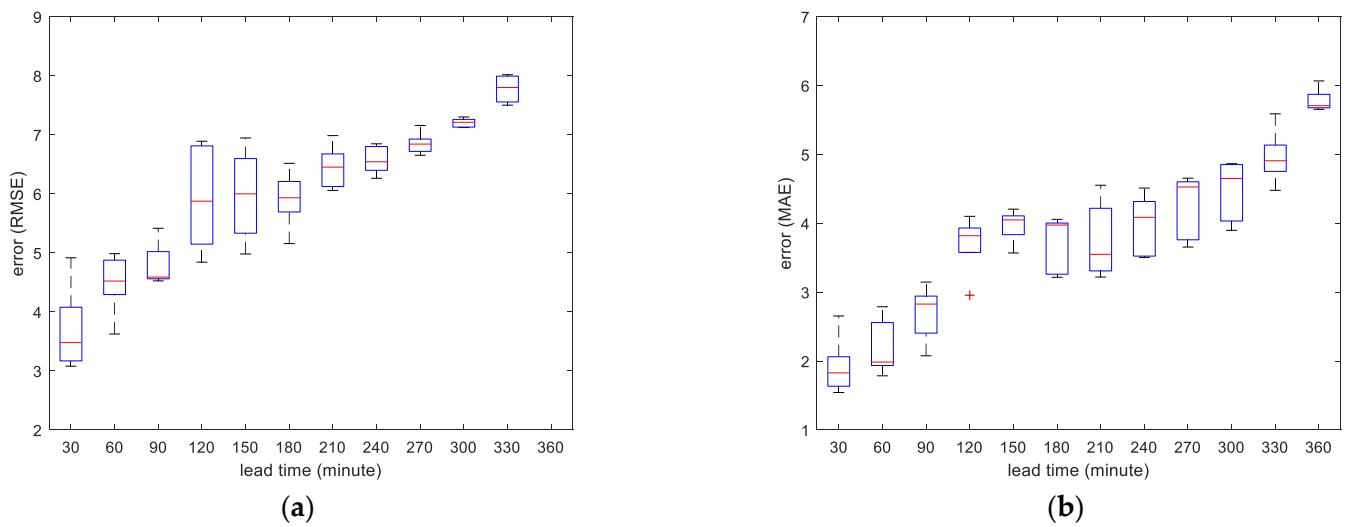


Figure 13. Cont.

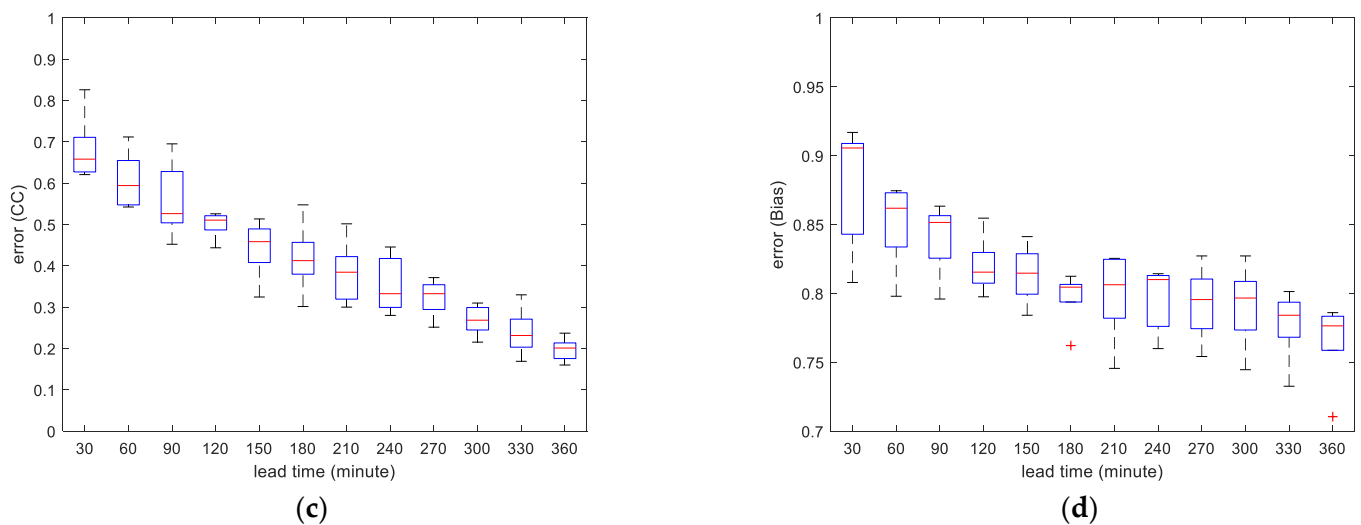


Figure 13. Box plot diagrams of ensemble precipitation nowcast skill as a function of lead time for averaged (a) root mean square error (b) mean absolute error; (c) correlation coefficient; and (d) BIAS metrics.

Each box plot presents four evaluation metrics. A similar pattern in the variations of RMSE and MAE, CC and BIAS with lead time was observed in the five precipitation events, although differing magnitudes are given. An asymptotic growth in MAE and an asymptotic reduction in CC with higher lead time was found. For smaller lead times for the four metrics, generally the spread box is larger. Plus, since the values of CC less than 0.5 after the lead time becomes 120 min, the quality of precipitation nowcasting by using the GPM data is high before 120 min. When the lead time reaches 120 min, the errors of nowcasts increase rapidly. So, the GPM IMERG precipitation data is satisfying for real-time short-term nowcasting, particular for two hours ahead.

7. Conclusions and Summary

In conclusion, the quality of the GPM IMERG precipitation product at half-hour and 0.1° resolution was evaluated, using daily precipitation observation data from over 2800 rain gauges across Mexico as reference. The STEPS model was applied to explore the potential of the GPM IMERG precipitation product for real-time short-time precipitation nowcasting (forecasting) in this analysis. The analysis was divided into two parts: the first part used rain gauge data as a reference for data quality evaluation, while the second part evaluated the GPM IMERG data. Five events were selected, and the data was applied in the STEPS model to present the nowcasting performance over a relatively short lead time period of 0–6 h. The main conclusions of this study are as follows.

(1) The quality of the GPM IMERG precipitation product at annual and national scales was investigated. The performance of the data was represented by several evaluation metrics, which were RMSE, CC, MAE, BIAS, POD, FAR and CSI. It was found that the GPM IMERG precipitation product showed a slight underestimation over Mexico, with small BIAS evaluations of -7.37% and -6.87% for the annual scale and national scale, respectively, and that fluctuations between over and underestimating at the daily scale were due to precipitation intensity and latitude. The quality of GPM IMERG data improved at the national scale, with the lowest estimated error.

(2) The GPM IMERG product is able to reproduce a mostly consistent distribution of precipitation at the annual scale. The overall results show the GPM precipitation data in high agreement with the data from the rain gauges and provides better precipitation observations in remote areas, with great CC and POD values.

(3) The nowcasting model was applied to explore the potential of GPM precipitation data for precipitation real-time short-term nowcasting and forecasting. The performance of precipitation nowcasting was examined by the RMSE, CC, BIAS and MAE metrics. The

errors between the STEPS nowcasts and GPM observed precipitation were estimated and plotted. Results from a comparison of each event showed qualitatively similar trends. The accuracy and quality of precipitation nowcasting generally decreased as the lead time increased, and the nowcasting quality reduced rapidly when the lead time reached 120 min ($CC < 0.5$). Therefore, the precipitation nowcasting performance by using GPM data is acceptable in Mexico beyond 2 h, after which the errors in the forecasts tend to increase very rapidly.

8. Future Studies and Shortcomings

For future studies, the quality of IMERG should be improved to provide more precise half-hourly precipitation estimates, especially for territories with dry climates, as well as high latitudes and altitudes. Correspondingly, more studies are required to assess the performance of GPM IMERG against other satellite and reanalysis products to find the advantages and limitations of the GPM satellite. Furthermore, other precipitation specific properties such as spatial and temporal heterogeneity, spatial and temporal intermittence, extreme variability and multi-fractal comparisons is necessary to overcome substantial uncertainties rainfall estimations [57–59]. Cristiano et al. [60] also depicted in their review that the rainfall variability may need wider range of conditions and scenario based in observational datasets for urban hydrological basins, which need proper analysis for development of better hydrological response system with higher sensitivity.

For nowcasting, in order to obtain better precipitation nowcasting results, the precipitation data of GPM IMERG product and rain gauge can be blended, such as kriging with external drift and the double-kernel smoothing methods. The characteristics of uncertainty and error of new generation of geosynchronous satellite products launched by the National Aeronautics and Space Administration (NASA) as GPM IMERG and National Oceanic and Atmospheric Administration (NOAA) will open new perspective for nowcasting and data assimilation. Moreover, such products should be further explored to encourage the application and development of products such as IMERG and geostationary lightning mapper sensors, respectively, and their associative algorithms in the recent era. This forecasting technique is extremely important especially for issuing flash flood warnings several hours in advance. Heavy rainfall is especially frequent in the Yangtze River delta area of southern China. In the future, more case studies can be conducted in this area in order to enhance the accuracy of nowcasting and forecasting precipitation models.

Supplementary Materials: The following are available online at <https://www.mdpi.com/article/10.3390/w13101422/s1>, Figure S1. Precipitation on 22 October 2015 at 9:30, based on (a) GPM estimated precipitation and (b) 30-min forecast precipitation from STEPS precipitation nowcast, Figure S2. Precipitation on 22 October 2015 at 10:00, based on (a) GPM estimated precipitation and (b) 30-min forecast precipitation from STEPS precipitation nowcast, Figure S3. Precipitation on 22 October 2015 at 10:30, based on (a) GPM estimated precipitation and (b) 30-min forecast precipitation from STEPS precipitation nowcast, Figure S4. Precipitation on 22 October 2015 at 11:00, based on (a) GPM estimated precipitation and (b) 30-min forecast precipitation from STEPS precipitation nowcast, Figure S5. Precipitation on 22 October 2015 at 11:30, based on (a) GPM estimated precipitation and (b) 30-min forecast precipitation from STEPS precipitation nowcast, Figure S6. Precipitation on 22 October 2015 at 12:00, based on (a) GPM estimated precipitation and (b) 30-min forecast precipitation from STEPS precipitation nowcast, Figure S7. Precipitation on 22 October 2015 at 12:30, based on (a) GPM estimated precipitation and (b) 30-min forecast precipitation from STEPS precipitation nowcast, Figure S8. Precipitation on 22 October 2015 at 13:00, based on (a) GPM estimated precipitation and (b) 30-min forecast precipitation from STEPS precipitation nowcast, Figure S9. Precipitation on 22 October 2015 at 13:30, based on (a) GPM estimated precipitation and (b) 30-min forecast precipitation from STEPS precipitation nowcast, Figure S10. Precipitation on 22 October 2015 at 14:00, based on (a) GPM estimated precipitation and (b) 30-min forecast precipitation from STEPS precipitation nowcast, Figure S11. Precipitation on 22 October 2015 at 14:30, based on (a) GPM estimated precipitation and (b) 30-min forecast precipitation from STEPS precipitation nowcast.

Author Contributions: Conceptualization: K.W., P.S., Z.Y., J.H., L.K., F.G., X.T., and Y.X.; methodology: K.W., P.S., Z.Y., J.H., and X.T.; investigation: K.W., P.S., and Z.Y.; writing—original draft preparation: K.W., P.S., and Z.Y.; writing—review and editing: K.W., P.S., Z.Y., J.H., L.K., F.G., and X.T.; supervision: J.H., X.T., F.G., and Y.X.; funding acquisition: J.H., L.K., X.T., and Y.X. and Z.Y. All authors have read and agreed to the published version of the manuscript.

Funding: The authors acknowledge the support given by the Research Fund (RDH-101-2020-0044) of Xi'an Jiaotong-Liverpool University Urban and Environmental Studies University Re-search Center.

Institutional Review Board Statement: Not applicable.

Informed Consent Statement: Not applicable.

Data Availability Statement: The data presented in this study are available on request from the corresponding author.

Acknowledgments: We would like to thank Miguel A Rico-Ramirez for his helpful suggestions and data support in this study. Gratitude is also due to the Optimizing Water Streams Project funded by the Research Centre, Xi'an Jiaotong-Liverpool University.

Conflicts of Interest: The authors declare no conflict of interest.

References

- Kidd, C.; Huffman, G. Global precipitation measurement. *Meteorol. Appl.* **2011**, *18*, 334–353. [CrossRef]
- Ebert, E.E.; Janowiak, J.E.; Kidd, C. Comparison of Near-Real-Time Precipitation Estimates from Satellite Observations and Numerical Models. *Bull. Am. Meteorol. Soc.* **2007**, *88*, 47–64. [CrossRef]
- Nashwan, M.S.; Shahid, S.; Wang, X. Assessment of satellite-based precipitation measurement products over the hot desert climate of Egypt. *Remote Sens.* **2019**, *11*, 555. [CrossRef]
- Hamada, A.; Takayabu, Y.N.; Liu, C.; Zipser, E.J. Weak linkage between the heaviest rainfall and tallest storms. *Nat. Commun.* **2015**, *6*, 6213. [CrossRef]
- Liu, Z.; Ostrenga, D.; Teng, W.; Kempler, S. Tropical Rainfall Measuring Mission (TRMM) Precipitation Data and Services for Research and Applications. *Bull. Am. Meteorol. Soc.* **2012**, *93*, 1317–1325. [CrossRef]
- Wang, Z.; Zhong, R.; Lai, C.; Chen, J. Evaluation of the GPM IMERG satellite-based precipitation products and the hydrological utility. *Atmos. Res.* **2017**, *196*, 151–163. [CrossRef]
- NASA (The National Aeronautics and Space Administration). NASA. Global Precipitation Measurement. Available online: https://www.nasa.gov/mission_pages/GPM/spacecraft/index.html (accessed on 24 July 2019).
- Iguchi, T. Dual-Frequency Precipitation Radar (DPR) on the Global Precipitation Measurement (GPM) Mission's Core Observatory. In *Satellite Precipitation Measurement*; Springer: Cham, Switzerland, 2020; pp. 183–192.
- Prakash, S.; Mitra, A.K.; AghaKouchak, A.; Liu, Z.; Norouzi, H.; Pai, D.S. A preliminary assessment of GPM-based multi-satellite precipitation estimates over a monsoon dominated region. *J. Hydrol.* **2018**, *556*, 865–876. [CrossRef]
- Wu, Z.; Zhang, Y.; Zhang, L.; Hao, X.; Lei, H.; Zheng, H. Validation of GPM Precipitation Products by Comparison with Ground-Based Parsivel Disdrometers over Jianghuai Region. *Water* **2019**, *11*, 1260. [CrossRef]
- Tang, G.; Clark, M.P.; Papalexiou, S.M.; Ma, Z.; Hong, Y. Have satellite precipitation products improved over last two decades? A comprehensive comparison of GPM IMERG with nine satellite and reanalysis datasets. *Remote Sens. Environ.* **2020**, *240*, 111697. [CrossRef]
- Huffman, G.J.; Bolvin, D.T.; Braithwaite, D.; Hsu, K.; Joyce, R.; Kidd, C.; Nelkin, E.J.; Sorooshian, S.; Tan, J.; Xie, P. NASA Global Precipitation Measurement (GPM) Integrated Multi-satellitE Retrievals for GPM (IMERG). In *Algorithm Theoretical Basis Document (ATBD)*; NASA/GSFC: Greenbelt, MD, USA, 2019.
- Chen, X.; Long, D.; Hong, Y.; Zeng, C.; Yan, D.H. Improved modeling of snow and glacier melting by a progressive two-stage calibration strategy with GRACE and multisource data: How snow and glacier meltwater contributes to the runoff of the Upper Brahmaputra River basin? *Water Resour. Res.* **2017**, *53*, 2431–2466. [CrossRef]
- Gilewski, P.; Nawalany, M. Inter-Comparison of Rain-Gauge, Radar, and Satellite (IMERG GPM) Precipitation Estimates Performance for Rainfall-Runoff Modeling in a Mountainous Catchment in Poland. *Water* **2018**, *10*, 1665. [CrossRef]
- Shi, X.J.; Chen, Z.; Wang, H.; Yeung, D.Y.; Wong, W.K.; Woo, W.C. Convolutional LSTM network: A machine learning approach for precipitation nowcasting. *arXiv* **2015**, arXiv:1506.04214v2.
- Spyrou, C.; Varlas, G.; Pappa, A.; Mentzafou, A.; Katsafados, P.; Papadopoulos, A.; Anagnostou, M.N.; Kalogiros, J. Implementation of a Nowcasting Hydrometeorological System for Studying Flash Flood Events: The Case of Mandra, Greece. *Remote Sens.* **2020**, *12*, 2784. [CrossRef]
- Jeong, C.H.; Kim, W.; Joo, W.; Jang, D.; Yi, M.Y. Enhancing the Encoding-Forecasting Model for Precipitation Nowcasting by Putting High Emphasis on the Latest Data of the Time Step. *Atmosphere* **2021**, *12*, 261. [CrossRef]
- Tran, Q.K.; Song, S.K. Computer vision in precipitation nowcasting: Applying image quality assessment metrics for training deep neural networks. *Atmosphere* **2019**, *10*, 244. [CrossRef]

19. Deng, Y.C.; Hwang, J.H.; Lyu, Y.D. Developing Real-Time Nowcasting System for Regional Landslide Hazard Assessment under Extreme Rainfall Events. *Water* **2021**, *13*, 732. [[CrossRef](#)]
20. Liguori, S.; Rico-Ramirez, M.A. A review of current approaches to radar-based quantitative precipitation forecasts. *Int. J. River Basin Manag.* **2014**, *12*, 391–402. [[CrossRef](#)]
21. Johannsen, L.L.; Zambon, N.; Strauss, P.; Dostal, T.; Neumann, M.; Zumd, D.; Cochrane, T.A.; Blöschl, G.; Klik, A. Comparison of three types of laser optical disdrometers under natural rainfall conditions. *Hydrol. Sci. J.* **2020**, *65*, 524–535. [[CrossRef](#)]
22. Zhang, A.; Xiao, L.; Min, C.; Chen, S.; Kulie, M.; Huang, C.; Liang, Z. Evaluation of latest GPM-Era high-resolution satellite precipitation products during the May 2017 Guangdong extreme rainfall event. *Atmos. Res.* **2019**, *216*, 76–85. [[CrossRef](#)]
23. Sokol, Z.; Szturc, J.; Orellana-Alvear, J.; Popová, J.; Jurczyk, A.; Céleri, R. The Role of Weather Radar in Rainfall Estimation and Its Application in Meteorological and Hydrological Modelling—A Review. *Remote Sens.* **2021**, *13*, 351. [[CrossRef](#)]
24. Dandridge, C.; Lakshmi, V.; Bolten, J.; Srinivasan, R. Evaluation of Satellite-Based Rainfall Estimates in the Lower Mekong River Basin (Southeast Asia). *Remote Sens.* **2019**, *11*, 2709. [[CrossRef](#)]
25. Ciach, G.J.; Krajewski, W.F.; Anagnostou, E.N.; Baeck, M.L.; Smith, J.A.; McCollum, J.R.; Kruger, A. Radar rainfall estimation for ground validation studies of the Tropical Rainfall Measuring Mission. *J. Appl. Meteorol.* **1997**, *36*, 735–747. [[CrossRef](#)]
26. Habib, E.; Krajewski, W.F. Uncertainty Analysis of the TRMM Ground-Validation Radar-Rainfall Products: Application to the TEFLUN-B Field Campaign. *J. Appl. Meteorol.* **2002**, *41*, 558–572. [[CrossRef](#)]
27. Steiner, M.; Smith, J.A.; Burges, S.J.; Alonso, C.V.; Darden, R.W. Effect of bias adjustment and rain gauge data quality control on radar rainfall estimation. *Water Resour. Res.* **1999**, *35*, 2487–2503. [[CrossRef](#)]
28. Sypka, P. Dynamic real-time volumetric correction for tipping-bucket rain gauges. *Agric. For. Meteorol.* **2019**, *271*, 158–167. [[CrossRef](#)]
29. Mahmud, M.; Mohd Yusof, A.A.; Mohd Reba, M.N.; Hashim, M. Mapping the Daily Rainfall over an Ungauged Tropical Micro-Watershed: A Downscaling Algorithm Using GPM Data. *Water* **2020**, *12*, 1661. [[CrossRef](#)]
30. Cai, Y.; Jin, C.; Wang, A.; Guan, D.; Wu, J.; Yuan, F.; Xu, L. Spatio-temporal analysis of the accuracy of tropical multisatellite precipitation analysis 3B42 precipitation data in mid-high latitudes of China. *PLoS ONE* **2015**, *10*, e0120026.
31. Mazzoglio, P.; Laio, F.; Balbo, S.; Boccardo, P.; Disabato, F. Improving an Extreme Rainfall Detection System with GPM IMERG data. *Remote Sens.* **2019**, *11*, 677. [[CrossRef](#)]
32. Cao, Q.; Hong, Y.; Qi, Y.; Wen, Y.; Zhang, J.; Gourley, J.J.; Liao, L. Empirical conversion of the vertical profile of reflectivity from Ku-band to S-band frequency. *J. Geophys. Res. Atmos.* **2013**, *118*, 1814–1825. [[CrossRef](#)]
33. Du, L.; Tian, Q.; Yu, T.; Meng, Q.; Jancso, T.; Udvardy, P.; Huang, Y. A comprehensive drought monitoring method integrating MODIS and TRMM data. *Int. J. Appl. Earth Obs. Geoinf.* **2013**, *23*, 245–253. [[CrossRef](#)]
34. Yatagai, A.; Krishnamurti, T.N.; Kumar, V.; Mishra, A.K.; Simon, A. Use of APHRODITE Rain Gauge-Based Precipitation and TRMM 3B43 Products for Improving Asian Monsoon Seasonal Precipitation Forecasts by the Superensemble Method. *J. Clim.* **2014**, *27*, 1062–1069. [[CrossRef](#)]
35. Qin, J.; Chen, Z.; Yang, K.; Liang, S.; Tang, W. Estimation of monthly-mean daily global solar radiation based on MODIS and TRMM products. *Appl. Energy* **2011**, *88*, 2480–2489. [[CrossRef](#)]
36. Prakash, S.; Mitra, A.K.; Pai, D.S.; AghaKouchak, A. From TRMM to GPM: How well can heavy rainfall be detected from space? *Adv. Water Resour.* **2016**, *88*, 1–7. [[CrossRef](#)]
37. Arshad, M.; Ma, X.; Yin, J.; Ullah, W.; Ali, G.; Ullah, S.; Liu, M.; Shahzaman, M.; Ullah, I. Evaluation of GPM-IMERG and TRMM-3B42 precipitation products over Pakistan. *Atmos. Res.* **2020**, *249*, 105341. [[CrossRef](#)]
38. Wu, Y.; Zhang, Z.; Huang, Y.; Jin, Q.; Chen, X.; Chang, J. Evaluation of the GPM IMERG v5 and TRMM 3B42 v7 precipitation products in the Yangtze River basin, China. *Water* **2019**, *11*, 1459. [[CrossRef](#)]
39. Sun, Q.; Miao, C.; Duan, Q.; Ashouri, H.; Sorooshian, S.; Hsu, K.L. A review of global precipitation data sets: Data sources, estimation, and intercomparisons. *Rev. Geophys.* **2018**, *56*, 79–107. [[CrossRef](#)]
40. Bowler, N.E.; Pierce, C.E.; Seed, A.W. STEPS: A probabilistic precipitation forecasting scheme which merges an extrapolation nowcast with downscaled NWP. *Q. J. R. Meteorol. Soc. J. Atmos. Sci. Appl. Meteorol. Phys. Oceanogr.* **2006**, *132*, 2127–2155. [[CrossRef](#)]
41. Seed, A.W.; Pierce, C.E.; Norman, K. Formulation and evaluation of a scale decomposition-based stochastic precipitation nowcast scheme. *Water Resour. Res.* **2013**, *49*, 6624–6641. [[CrossRef](#)]
42. Liguori, S.; Rico-Ramirez, M.A.; Schellart, A.N.A.; Saul, A.J. Using probabilistic radar rainfall nowcasts and NWP forecasts for flow prediction in urban catchments. *Atmos. Res.* **2012**, *103*, 80–95. [[CrossRef](#)]
43. Lewis, H.; Mittermaier, M.; Mylne, K.; Norman, K.; Scaife, A.; Neal, R.; Pierce, C.; Harrison, D.; Jewell, S.; Kendon, M.; et al. From months to minutes—exploring the value of high-resolution rainfall observation and prediction during the UK winter storms of 2013/2014. *Meteorol. Appl.* **2015**, *22*, 90–104. [[CrossRef](#)]
44. National Water Commission (CONAGUA). Statistics on Water in Mexico. Available online: <https://www.nwcjamaica.com/> (accessed on 31 July 2019).
45. Sámano-Romero, G.; Mautner, M.; Chávez-Mejía, A.; Jiménez-Cisneros, B. Assessing marginalized communities in Mexico for implementation of rainwater catchment systems. *Water* **2016**, *8*, 140. [[CrossRef](#)]
46. Naik, B.; Khatua, K.K.; Wright, N.; Sleigh, A.; Singh, P. Numerical modeling of converging compound channel flow. *ISH J. Hydraul. Eng.* **2018**, *24*, 285–297. [[CrossRef](#)]

47. Singh, P.K.; Banerjee, S.; Naik, B.; Kumar, A.; Khatua, K.K. Lateral distribution of depth average velocity & boundary shear stress in a gravel bed open channel flow. *ISH J. Hydraul. Eng.* **2018**, *27*, 1–15. [[CrossRef](#)]
48. Singh, P.K.; Khatua, K.K. Lateral dissemination of depth-averaged velocity, boundary shear stress and stage-discharge curves for compound channels. *ISH J. Hydraul. Eng.* **2018**, 1–14. [[CrossRef](#)]
49. Tang, G.; Ma, Y.; Long, D.; Zhong, L.; Hong, Y. Evaluation of GPM Day-1 IMERG and TMPA Version-7 legacy products over Mainland China at multiple spatiotemporal scales. *J. Hydrol.* **2016**, *533*, 152–167. [[CrossRef](#)]
50. Chen, C.; Chen, Q.; Duan, Z.; Zhang, J.; Mo, K.; Li, Z.; Tang, G. Multiscale Comparative Evaluation of the GPM IMERG v5 and TRMM 3B42 v7 Precipitation Products from 2015 to 2017 over a Climate Transition Area of China. *Remote Sens.* **2018**, *10*, 944. [[CrossRef](#)]
51. Sharifi, E.; Steinacker, R.; Saghafian, B. Assessment of GPM-IMERG and Other Precipitation Products against Gauge Data under Different Topographic and Climatic Conditions in Iran: Preliminary Results. *Remote Sens.* **2016**, *8*, 135. [[CrossRef](#)]
52. Yong, B.; Ren, L.L.; Hong, Y.; Wang, J.H.; Gourley, J.J.; Jiang, S.H.; Chen, X.; Wang, W. Hydrologic evaluation of Multisatellite Precipitation Analysis standard precipitation products in basins beyond its inclined latitude band: A case study in Laohahe basin, China. *Water Resour. Res.* **2010**, *46*. [[CrossRef](#)]
53. Libertino, A.; Sharma, A.; Lakshmi, V.; Claps, P. A global assessment of the timing of extreme rainfall from TRMM and GPM for improving hydrologic design. *Environ. Res. Lett.* **2016**, *11*, 054003. [[CrossRef](#)]
54. PC, S.; Misumi, R.; Nakatani, T.; Iwanami, K.; Maki, M.; Seed, A.W.; Hirano, K. Comparison of rainfall nowcasting derived from the STEPS model and JMA precipitation nowcasts. *Hydrol. Res. Lett.* **2015**, *9*, 54–60.
55. Foresti, L.; Seed, A. On the spatial distribution of rainfall nowcasting errors due to orographic forcing. *Meteorol. Appl.* **2015**, *22*, 60–74. [[CrossRef](#)]
56. Omranian, E.; Sharif, H.; Tavakoly, A. How Well Can Global Precipitation Measurement (GPM) Capture Hurricanes? Case Study: Hurricane Harvey. *Remote Sens.* **2018**, *10*, 1150. [[CrossRef](#)]
57. Vendrasco, E.P.; Machado, L.A.; Araujo, C.S.; Ribaud, J.-F.; Ferreira, R.C. Potential use of the GLM for nowcasting and data assimilation. *Atmos. Res.* **2020**, *242*, 105019. [[CrossRef](#)]
58. Shehu, B.; Haberlandt, U. Relevance of merging radar and rainfall gauge data for rainfall nowcasting in urban hydrology. *J. Hydrol.* **2021**, *594*, 125931. [[CrossRef](#)]
59. Imhoff, R.O.; Brauer, C.C.; Overeem, A.; Weerts, A.H.; Uijlenhoet, R. Spatial and Temporal Evaluation of Radar Rainfall Nowcasting Techniques on 1,533 Events. *Water Resour. Res.* **2020**, *56*, e2019WR026723. [[CrossRef](#)]
60. Cristiano, E.; Veldhuis, M.C.T.; Giesen, N.V.D. Spatial and temporal variability of rainfall and their effects on hydrological response in urban areas—A review. *Hydrol. Earth Syst. Sci.* **2017**, *21*, 3859–3878. [[CrossRef](#)]